LIQUID PETROLEUM GAS FLAME IN A DOUBLE-SWIRL GAS TURBINE MODEL COMBUSTOR
Lean Blow-Out, Pollutant, Preheating

by

Amir MARDANI*, Hamed Rezapour RASTAAGHI, and Alireza Fazlollahi GHOMSHI

Department of Aerospace Engineering, Sharif University of Technology, Tehran, Iran

Original scientific paper
https://doi.org/10.2298/TSCI190623139M

In this paper, lean blow-out limits in a double swirl GT model combustor were investigated experimentally for liquid petroleum gas fuel. The lean blow-out curve was extracted for different combustor configurations. While burner could operate reasonably under ultra-lean conditions, two different sets of operating conditions, one with a low flow rate and another one with high flow rate, are identified and studied in terms of lean blow-out and pollutant. Results showed that while the flame structure was similar in both cases, the chamber responses to geometrical changes and also preheating are minimal at the low flow rate. That means confinement and injector type have desirable effects on stability borders but not for the low flow rate. The channeled injector shifted down the lean blow-out limit around 28% at high flow rate. Measurements on the combustor exhaust gas composition and temperature indicate a region with relatively complete combustion and reasonable temperature and a very low level of exhaust NO_x pollutants (i. e., below 10 ppm) at about 25-50% above the lean blow-out. In this operating envelope, a burner power increment led to a higher exhaust average temperature and combustion efficiency, while NO_x formation decreased. Preheating the inlet air up to 100 °C results in an improvement in burner stability in about 10%, but NO_x production intensifies more than three times. Results indicate that the lean blow-out limit is configured more by the burner design and aerodynamic aspects rather than the fuel type.

Key words: *liquid petroleum gas, swirl, GT combustor, preheat, lean blow-out*

Introduction

Many investigations are performing on gas turbine (GT) combustors in order to reduce pollutant formations and increase performance [1-6]. Investigations show that operating under lean premixed or partially premixed conditions can reduce emissions of NO_x and CO [7]. High swirl flames provide small size and high energy conversion chambers with reasonable mixing, ignition, and stability characteristics using concepts of vortex breakdown and strong inner recirculation [1, 3, 8]. Double swirl combustors with a high level of turbulence and heat release in small volume would be useful in terms of reducing residence time, flame stabilization, and ignition in a wide range of operating conditions [1]. These burner configurations could decrease the reliance on staging of the air-flow and, therefore, a size reduction of chamber favorably.

* Corresponding author, e-mail: amardani@sharif.edu

The German Aerospace Center (DLR) has established a GT model combustor named GTMC in which CH_4 is injected between two co-swirling air inlets. They have published a wide range of experimental reacting and non-reacting data for three specific operating conditions for CH_4 as fuel [6]. Flame A as a perfectly stable flame, operated at a specific power rate comparable to an aeronautical or modern aero-derivative industrial GT, flame B with strong thermo-acoustic noise chosen at a specific power rate comparable to most industrial GT; and flame C, with sudden partially extinction and reestablishment of stable process, operated at the same air-flow as flame B but with reduced fuel supply close to the lean extinction limit [1]. Most researches on GTMC are carried out under these particular operating conditions. The first time, GTMC was investigated experimentally by Duan *et al.* [9] in 2004 by laser-based measurements of flame C. They provided OH and CH PLIF, mean velocity field, and some other experimental data and concluded that the flow field exhibits a strong swirl-induced re-circulation zone with high-velocity fluctuations in the shear layers built by adjacent inlet flows. In 2005, Weigand *et al.* [10] investigated flame B for the mechanism of periodic combustion instability. They observed a lifted flame under a partially premixed mode. Their results showed that the oscillations of the heat release rate were accompanied by periodic changes in the thermal expansion, swirl intensity, and pressure, which in turn influenced the flow field. Beside them, Meier *et al.* [11] investigated the mixing, reaction progress, and flame front structures of flames A and B using laser diagnostics. They concluded that the flames were lifted and partially premixed before ignition with relatively low variations in mixture fraction compared to pure diffusion flames. In 2006, Weigand *et al.* [1], and Meira *et al.* [12] classified flames A, B, and C with respect to combustion instabilities, as mentioned before, and established a comprehensive database that can be used for validation and improvement of combustion models. In 2008, Sadanandan *et al.* [13] examined simultaneous measurement of the flow field and flame for a clear understanding of the underlying mechanisms at flame B. In 2009, Stohr *et al.* [14] investigated flame B and measured velocity fields and flame structures using simultaneous stereo-PIV and OH-PLIF. Sadanandan *et al.* [15] also investigated flame B and examined flow field-flame structure interactions. Boxx *et al.* [16] investigated flame B using high-speed laser imaging and presented the effects of both of processing vortex core (PVC) and thermo-acoustic pulsation on the flow field and the reaction zone. Another work by Boxx *et al.* [17] was investigated on flame B to describe an approach of imaging the dynamic interaction of the flame front and flow field. In 2010, Boxx *et al.* [18] presented observations and analysis of the time-dependent behavior of flame B. Steinberg *et al.* [19] carried out a detailed analysis of the flow–flame interactions associated with thermo-acoustic fluctuations of flame B. In 2011, Stohr *et al.* [20] studied flame C using chemiluminescence imaging and simultaneous stereo-PIV and OH-PLIF measurements. They investigated the stabilization mechanism of the flame, when it is close to the lean blow-out (LBO). They observed that the flame shape and flow field are very similar to fully stable operation (without intermediate blow-out events) at a slightly higher equivalence ratio than the LBO. They found out that near the LBO, there are essentially two regions where the reaction takes place, namely the helical zone along the PVC and the flame root around the lower stagnation point. Kutne *et al.* [21] carried out experiments on oxyfuel flames in GTMC. Their results showed a strong influence of the O_2 concentration on the combustion behavior in contrast to the equivalence ratio, which has only a one minimal effect. In 2012, Stohr *et al.* [7] studied the interaction of the helical PVC with the flame. Allison *et al.* [22, 23] investigated the acoustic behavior of GTMC using both synthetic gas and standard hydrocarbon fuels. In the framework of numerical studies on GTMC, there are also some reports: first in 2008, Windenhorn *et al.* [8] modeled the GTMC by a 3-D simulation using scale

adaptive simulation, detached eddy simulation, and Reynolds-averaged Navier Stokes (RANS) approaches. In 2013, See and Ihme [2] modeled the GTMC using the large eddy simulation and reported sensitivity of modeling to subgrid-scale turbulence models and finally recommended the Verman subgrid model for GTMC [6]. Also, in 2016, Mardani *et al.* [6] modeled GTMC using two different turbulence-chemistry interaction models: the eddy dissipation concept and transported probability density function. Their modeling was performed by solving RANS and Reynolds stress model equations for a 2-D-axisymmetric computational domain accompanied by swirl. There are some other works on this combustor numerically and experimentally.

Following the literature indicates that there is little reported information about the most critical features of GTMC in terms of LBO and its pollutant for fuels other than CH_4. Furthermore, low level preheating of inlet air, which emulates heat recovery concept from the exhaust, is not reported according to our knowledge. On the other hand, the primary fuel of GTMC was CH_4, so the topics as mentioned earlier, are not considered for LPG fuel. So, we are going to investigate the redesigned version of GTMC, which is manufactured in Sharif University of Technology and called here SGTMC, using LPG as fuel, basically with focusing on the stability blow-out limit, the effect of preheating, and emissions which are less reported as our knowledge. Therefore, in this work, experimental investigation of the combustor was done for a wide range of air-flow rates and in terms of stability limit, flame direct photography, preheating effects, and emissions in a wide range of operating conditions of the SGTMC. Moreover, non-reacting flow field modeling of the burner, the same as done in the previous report of the author, has been done and used limitedly to get some more information about the flow field and for discussions [6]. This numerical modeling was not the main objective of this work and; therefore, it is eliminated to report due to lack of space.

Experimental set-up

Combustor characteristics

The GT model combustor is schematically shown in fig. 1. The burner is a reconstructed version of a model GT combustor for gaseous fuels [1, 8] (GTMC), which entitled here as Sharif GT model combustor (SGTMC). Dry air at atmospheric pressure and the room temperature was supplied to the combustor through a central nozzle with a diameter of 15 mm and an annular nozzle with a diameter of 17-25 mm with the same swirl direction. Both air inlets are fed from a common plenum with a diameter of 79 mm and a height of 72 mm. The radial swirls consisted of 8 and 12 channels for the central and annular nozzles, respectively. The LPG as fuel was fed through a 0.5 mm width path in the axial direction, using a perforated or simple annular slit according to the selected type of the injector, see fig. 1. The combustion chamber had a square section of 83×83 mm and a height of 112 mm with steel plates as walls. Furthermore, in some tests, a cylindrical quartz glass with a diameter of 90 mm is used as a chamber wall. A conical top plate, made of steel,

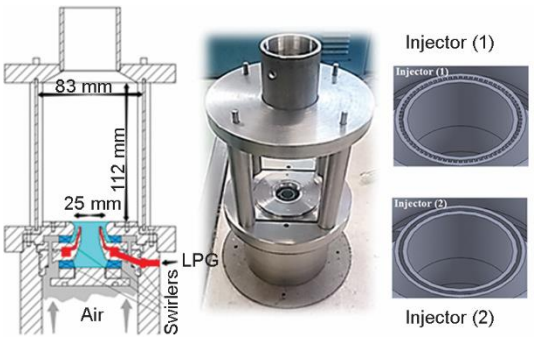

Figure 1. Schematic drawing of the model combustor (SGTMC) and schematic detailed view of fuel injectors

with a central exhaust tube, conducts the high-velocity gas to the exit and prevents backflow from outside [1]. In comparison with GTMC, SGTMC is different in combustion chamber size (83×83×112 mm^3 against 85×85×110 mm^3 in the DLR version), fuel injector flexible design, and steel plates as chamber walls instead of quartz plates, chamber geometry when the quartz cylinder is used as wall, and fuel type. In fig. 1, two used injectors are shown. One of the injectors performs the injection process via 72 channels (0.5×0.5 mm^2) arranged annularly between air inlets which is similar to the one used in GTMC, *i. e.*, Injector (1), and another one is in the form of a simple ring, *i. e.*, Injector (2), which is only used in SGTMC.

Moreover, inlet air preheating up to around 100 K by a controllable electrical heater is done in this work. It is worthy to say that to compare GTMC with SGTMC, some modeling was also done on SGTMC for CH_4 fuel and revealed that burners are the same with similar flow field structure inside the chamber.

Experimental facility and measuring techniques

The experimental facility is shown in fig. 2, schematically. We used a digital flow meter GPM-DC-M-B-1-1-5D22 and three rotameters for fuel- and air-flow rates under different operating conditions, while the corrections due to the fuel and air temperature and pressure have been considered through:

$$Q_{\text{actual}} = Q_{\text{calibrated}} \sqrt{\frac{P_{\text{actual}}}{P_{\text{calibrated}}} \frac{T_{\text{calibrated}}}{T_{\text{actual}}} \frac{M_{\text{calibrated}}}{M_{\text{actual}}}} \tag{1}$$

where subscripts *actual* and *calibrated* refer to real and read values in gages, respectively, T [K] – the gas-flow temperature, P – the static pressure of the flow, M – the gas molecular weight, and Q – the volumetric flow rate. The actual pressure and temperature for air-flow line were, respectively, 655 mmHg and 299-302.5 K, and they were 654 mmHg and 285-311.15 K for the fuel line, respectively.

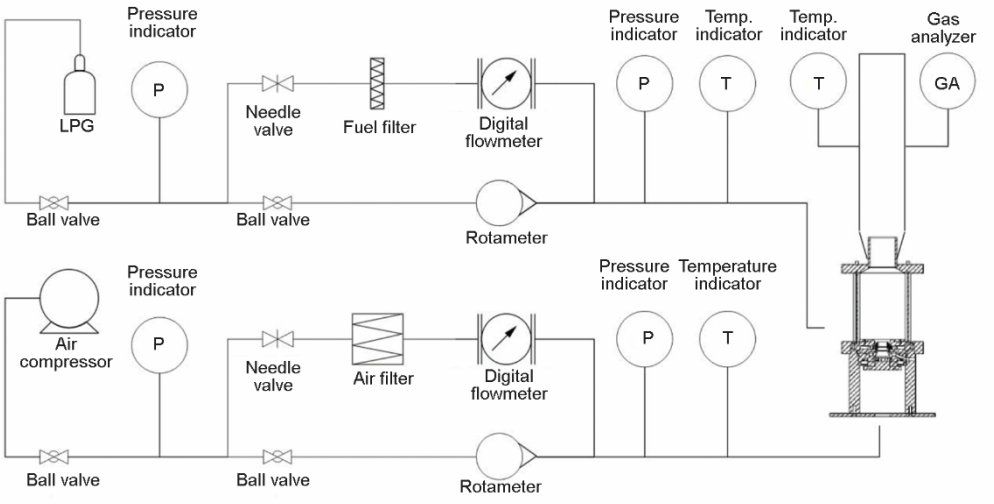

Figure 2. Schematic drawing of the experimental set-up

To achieve the LBO in terms of equivalence ratio *vs.* total flow rate, LPG + air in m^3 per hour, some tests were done through two different procedures. For low flow rates (LFR), we

kept fuel-flow rate constant and increased air-flow until the flame blows out, while for high flow rates (HFR), the fuel-flow rate was decreased in a constant air-flow rate until the flame blows out. For repeatability of the results, each test was done three times. Nikon D7100 camera was used for flame direct photography and KIMO (KIGAZ 300) gas analyzer for the measurements of the exhaust gas species and temperature.

Results and discussions

In this section, the results of the experimental investigation of LPG-air in SGTMC combustor are presented. In this way, it is aimed to present some results regarding the capability of SGTMC in flame stabilization and reducing exhaust pollutants. The first section presents the flame stabilization behavior and lean stability limits graphs for four various burner-chamber configurations in terms of confinement and injector type. The second section is going to analyze some flame pictures in various operating conditions. The third section would present some exhaust gases analysis to achieve the region with the best efficiency in terms of stability and pollutant. Finally, in the last section, the effect of air preheating on LBO and NO_x formation is investigated.

Flame stabilization behavior

The effects of chamber confinement and injector configuration on the burner lean stability limit are followed in this section. So, measurements are considered for the burner with the chamber walls and without them (*i. e.*, in the free atmosphere). Also, for each chamber configuration, two fuel injectors are tested. Figure 3 shows the LBO curves for the four mentioned different conditions. In this figure, the equivalence ratio *vs.* total flow rate (*i. e.*, $Q_{LPG} + Q_{air}$) is used to show LBO of LPG fuel. Furthermore, two reported LBO limits of GTMC burner for CH_4 as fuel are illustrated in the figure from reports of Weigand *et al.* [1] and Allison [22, 23]. For more detailed analysis, the stability graph is partitioned into two sections wherever various LBO profiles are going away from each other. The region with 0 to 6 m^3 per hour flow rate was named as LFR region, and the region with more than 6 m^3 per hour flow rate was named HFR region. Before discussing the LBO profiles, it would be worthy of mentioning if these two regions are compared in terms of flow field structure. Due to the lack of our experimental facilities, the numerical method could be helpful. In present work, only some limited results from modeling is used to help the discussions. Because of the lack of space, a detail description of modeling and prediction is eliminated from the main text, but they are available in [6].

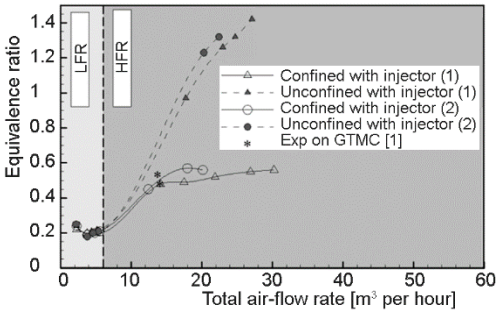

Figure 3. The LBO graphs in various combustor configurations in SGTMC; furthermore, the LBO values of confined GTMC burner with the Injector (1) and CH_4 fuel are presented from the measurements [1, 22, 23].

Non-reacting flow field structure modeling for LFR condition showed that the combustion chamber operation is in the range of high swirl flows similar to HFR. That means both cases show the occurrence of the vortex breakdown phenomenon and formation of inner re-circulation zone (IRZ) around the center line and outer re-circulation zone (ORZ) in the corners of the combustor. Moreover, re-circulation bubbles form as a result of sudden expansion at the end of the

annular air inlet's wall. Therefore, both LFR and HFR have the same main flow structures, although the velocity levels are higher for HFR. The importance of LFR operating points could be in relation to the procedure of burner start-up and for the HFR to the load conditions. In continuation, the LBO limits of the burner in the whole range of operation are examined.

According to fig. 3, confinement of the burner is very useful on its lean stability limit for the case of perforated injector, although this effect is not significant enough to be visible in the LFR zone. Confinement has improved the LBO limit of the combustion chamber up to 250% rather than the un-confinement one. Moreover, the perforated injector has also decreased LBO up to 28% in comparison with the simple round slit injector. As expected, the figure confirmed that confinement has been more effective at higher flow rates. Without confinement by increasing the air-flow rate, LBO stability limit marches to fuel-rich mixtures with equivalence ratio higher than 1.2, which means a high level of unburned (UHC). This could be attributed to the chamber wall contribution on gas re-circulation and also intensified vortex breakdown inside the flow field, which is a very important stability mechanism for high swirl flames. For a more in-depth analysis, variation of swirl number of both air inlets of the burner, *vs.* air mass-flow rate, are calculated in a plane at a distance of 1 mm from the exit of inlets by 3-D modeling of inlets in fig. 4. This figure shows that the swirl number would increase with flow rate in about 28% for outer swirler while is relatively constant in central swirler and in the HFR region. Thus, the vortex breakdown intensifying due to outer swirler will be more effective in the HFR region and it seems that the turning point in the stability profiles and in the border of LFR and HFR is the point that vortex breakdown will be pronounced more after that. It may be concluded that outer air-flow has a main role in the flow field configuration by increasing the flow rate. On the other hand, and according to our onsite observation, in the unconfined chamber, the flame will be closer to the burner base, and the LBO has shifted toward the higher equivalence ratios.

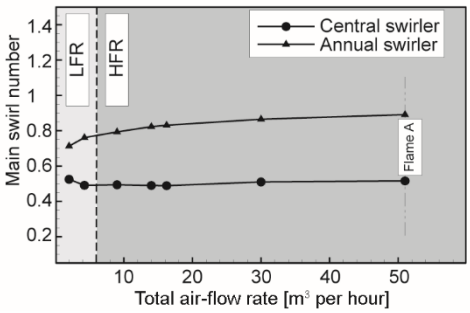

Figure 4. Calculated central and annular swirl numbers variations by the air-flow rate

Regarding the effect of fuel injector type on the LBO, it could be understood that the perforated injector, *i. e.*, Injector (1), has improved the LBO more than 20%. That means, it leads to run the burner in a stable mode at higher air-flow rates. By keeping in mind that the air inlets swirl numbers are not affected by injector type, this favorable effect of Injector (1) may be attributed to the higher local mixing at the grooves between the downstreams of fuel input channels and also jet-like injection of fuel through many channels, but it needs an accurate 3-D simulation to follow our guess. It is worthy to do a comparison between the LBO of the current burner, SGTMC, and based one, GTMC. Therefore, the reported lean extinctions values for GTMC burner are considered from the measurements of Weigand *et al.* [1] and Allison [22, 23]. The GTMC is configured for injector type (1) and CH_4 fuel under confinement conditions. Interestingly, there are a good compatibility between two burners operations regarding the LBO values, although they are run for two different fuels. Therefore, it may be inferred that the stability of the current kind of burner is more affected by its configuration and aerodynamic aspects rather than the fuel type. In this framework the results of current work may be useful for the other gaseous similar fuels.

Flame direct photography

To have a visual view on the flame structure of SGTMC, different kinds of flames of the current burner are considered here at first, and in continuation, the flame response to the air mass-flow rate is followed in terms of flame zone photos. It should be mentioned that due to the *oscillatory behavior* of flames, quantitative analysis of flame shape should be based on an average of enough number of images, in a sequence, in order to reflect steady-state behavior. This issue has been considered by increasing the camera exposure time to reach an appropriate photo, which is similar between different shots. This exposure time is 1/160 seconds.

For the first part, two operating conditions, according to tab. 1, are selected for direct photography. To analyze the flame pictures, some flame parameters such as flame surface, width, height, and flame root angle are defined.

Table 1. Operating conditions of analyzed flame pictures (section *Flame direct photography*)

Region	Q_{Air} [m^3 per hour]	Q_{LPG} [m^3 per hour]	Fuel mixture*	Φ_{global}	T [K]
LFR	4.24	0.034	30% C_3H_8, 70% C_4H_{10}	0.23	298
HFR	16.17	0.86	30% C_3H_8, 70% C_4H_{10}	1.5	298

* Volume basis

In fig. 5, two photos are exhibited for the operating condition in the LFR region, one for the confined burner and another one for the unconfined case. It can be seen that the flame is lifted in which high intense reaction regions are in the distance from the base of the chamber and also walls under confinement condition. Interestingly, flame photos showed a distribution of hot regions with various luminosities under oscillatory behavior according to our observations. If the blue regions are considered as high intense reaction zones, they seem to be distributed in a ring around the burner axis. Photos illustrate that the flame root angle for both cases is about 38°; hence the area of the side view of the luminous zone is smaller and broader for confined one. To complete the discussion, all flame picture parameters are presented in tab. 2.

Table 2. Flame photos parameters

Region	Confinement	Root angle [°]	Height [mm]	Width [mm]	Side view area [mm^2]
LFR	Unconfined	38	21	36	510
	Confined	38	18	42	540
HFR	Unconfined	39	80	55	3200

As a whole, for the LFR zone, fig. 5 and stability graphs show that there is not any remarkable effect of confinement for LFR, as expected. For the HFR region, at first unconfined configuration was focused.

In fig. 6(a) is for a typical unconfined stable and lifted flame, selected from the HFR region, and fig. 6(b) is for the attached flame. As can be seen, for fig. 6(a), in comparison with LFR flames, the flame size as well as the intensity of reaction zone increases in all dimensions, as expected, but the flame root angle remains relatively constant. Generally, according to our onsite observation, the flame lift-off decreases by moving toward the stability limit and in a region very close to stability limit, and just before flame extinction, the flame suddenly attaches

to the burner base, as shown in fig. 6. This particular type of flame could be considered as an unstable flame that is damaging to the burner base.

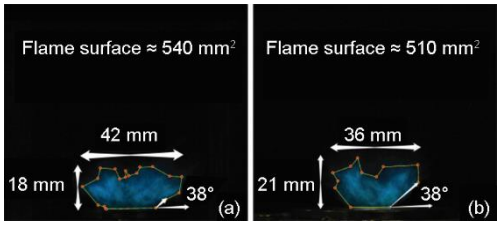

Figure 5. The LFR flame parameters based on tabs. 1 and 2; (a) unconfined, (b) confined, Injector (1)

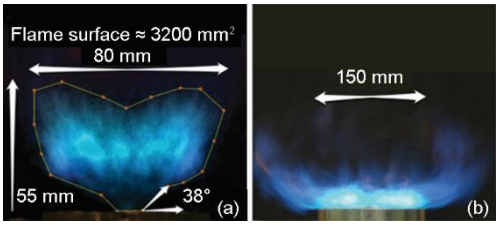

Figure 6. (a) The HFR flame parameters based on tabs. 1 and 2; (unconfined), (b) typical attached flame (unconfined), Injector (1)

Following previous discussions, the HFR condition under the confined chamber is considered in more detail by some images of the flame in the presence of a cylindrical quartz glass with a diameter of 90 mm in fig. 7. Four operating conditions of A_1 to A_4 are selected. For each photo, two different conditions are considered as camera settings for f-stop, exposure time, and ISO speed, which they are f/10, 1/160 seconds, and ISO 3200 as Set_1 and f/10, 1/5000 seconds, and Hi 2.0 as Set_2. Photos in the Set_1 group are visible to the naked eye, and Set_2 ones are considered for capturing the brightest areas of each photo.

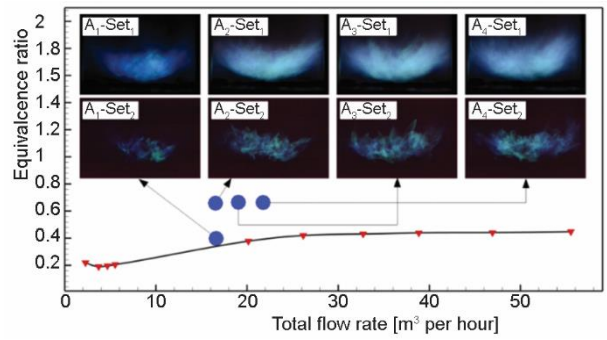

Figure 7. Flame photos of the confined burner for different operating conditions

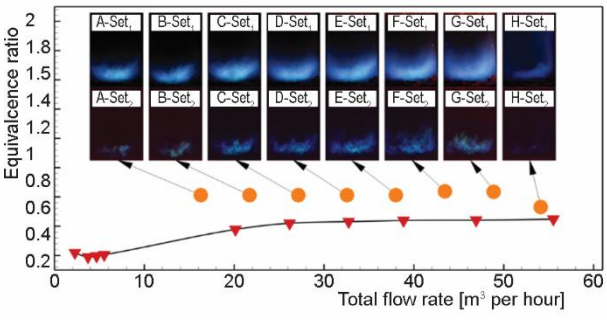

Figure 8. Flame photos of the confined burner in a wide range of operation (90 mm quartz tube)

The arrangement of photos in fig. 7 is based on the location of each of the operating conditions according to the LBO graph. If the Set_2 photos are assumed as the regions which correlate with the highest intensity of reactions or the highest level of energy release and optical radiation, it is observed that this region becomes wider by increasing the overall equivalence ratio and increasing the flow rate. Following the reports of Williams *et al.* [24] and Lu *et al.* [25], it may be inferred that the flame image correlates with the reaction zone. In the case of A_1 and A_2, the increase in brightness is due to the increment of equivalence ratio and so thermal power. In the case of A_2, A_3, and A_4, the increment in total flow rate and intensifying turbulence-combustion interactions could be a reason. In fig. 8, a series of flame

photos in the HFR region have been provided for different operating conditions with the same equivalence ratios. As can be seen, flame images are brighter by increasing the inlet reactant flow rate. This is because of more inlet fuel, which means more thermal power. Flame H, which operates near the LBO, has less flame front side-surface and brightness than the others. This could be attributed to the extensive local extinction in the reaction zone.

Overly, flame photos analysis show that reactions zone includes cloudy like reaction zones with different and distributed luminosity, and not an intense reaction region, which configured by the aerodynamics of burner. Under HFR condition, burner walls could be considered affective on the flame shape, although it seems that in the LFR region and during the starting procedure, the chamber walls are not so effective.

Exhaust emissions

In this section, the performance of the combustion chamber is studied in terms of exhaust gas composition, temperature, and pollutants. Sampling and measurement were only done for the confined burner with Injector (1) configuration. The concentrations of CH_4, CO, NO_x, O_2, and temperature were measured for some operating conditions selected from the LBO graph to achieve a region with the best efficiency and the lowest amount of the pollutants. All measurements were performed at 38 cm after the conical exhaust plate and on the axis of a tube with a 6 cm diameter. In fig. 9(a), measured unburned CH_4 concentrations are depicted while the LBO curve is imposed on them. It can be seen that there is a considerable UHC at the outlet for especially the LFR region and close to the LBO. They may be attributed to the local extinction and escaping some UHC from the flame area. However, there are still operating points, especially at far enough from the LBO, in which the exhaust CH_4 concentration is zero. These points of operations are considered for the following analysis. According to the figure, in most operating conditions under the HFR condition, there is no CH_4 in the exhaust gas, and if the CO concentrations, in fig. 9(b), are considered besides, it may be concluded that for the HFR operating condition, combustion is almost complete. However, there is some inefficiency in combustion, especially for the LFR, where probably there is not such powerful effect of swirl-induced mixing process to eliminate UHC, but in HFR, significance of vortex breakdown and formation of strong re-circulation zones seems to be present according to ultra-low level of CO. To complete the discussion, O_2 concentration is shown in fig. 9(c). As can be understood, there is about 10% excess O_2 at the chamber outlet for all operating conditions around the LBO line. It is not surprising and could be a reason for complete combustion. For more information, fig. 9(d) presents related temperature values. The temperature increases with flow rate because of increasing reaction rates and operating power. It also increases for higher equivalence ratios when approaching to the near-stoichiometric mixture, as expected. Moreover, this figure shows that the outlet gas temperature is lower than 1000 °C, which is reasonable. On the other hand, the temperature level in the graph would be helpful for discussing about NO_x concentrations as follows. The NO_x concentrations in the exhaust are shown for various operating conditions in the stability graph, fig. 9(e). In the LFR region, measurements, in different operating conditions with the same equivalence ratio, show that NO_x decreases a little with an increasing flow rate. This is probably because of decreased local residence time in high temperature regions, and dilution resulted from high re-circulation. In this region, for a constant total flow rate, the overall mixture becomes less lean by approaching the stoichiometric limit, so temperature increases, as shown in fig. 9(d), and leads to higher NO_x formation. In the HFR region, NO_x formation is reduced in comparison with the LFR zone, although the exhaust gas temperature is increased. In this region, generally with an increasing the total flow rate in a constant equivalence ratio,

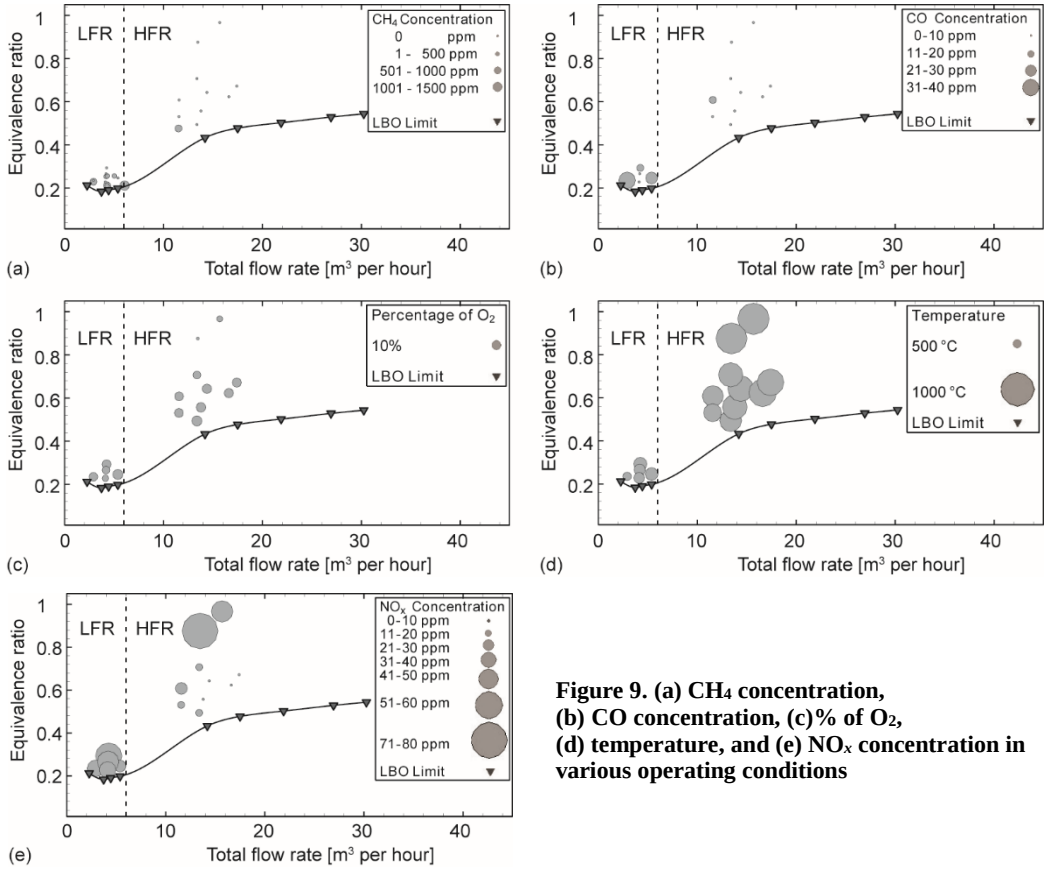

Figure 9. (a) CH_4 concentration, (b) CO concentration, (c)% of O_2, (d) temperature, and (e) NO_x concentration in various operating conditions

NO_x formation decreases to a very low level, probably as a result of decreased residence time in the high temperature regions. Moreover, by increasing the overall equivalence ratio in a constant flow rate, NO_x formation increases as temperature increases. It should be worthy to notice that the NO_x level is in a range below 80 ppm in the focused operating conditions and even ten ppm in many of them which could be a good reason for many researches on this burner, although, at the region very close to the LBO, it is hard to speak about level of emissions because of local extinctions and unsteady behavior of the flame. To go to a more detail description of burner behavior, measured data in fig. 9 are depicted in fig. 10(a) quantitatively, and also a linear curve fitting is done to extract the data behaviors. In this figure, variations of exhaust temperature, CH_4, CO, O_2, NO_x, and overall equivalence ratio of the chamber are shown *vs.* the total flow rate. The figure shows that in measured operating conditions, the overall equivalence ratio increases by total flow rate increment while excess O_2 decreases toward to about 10%. That is compatible with the overall behavior of GT combustors stability graphs. As can be understood from the graph, exhaust temperature has increased by total flow rate, and CH_4 and CO concentrations have decreased. This also indicates that combustion has been more completed for HFR, while NO_x formation has also decreased. It is an advantage of this burner in which power and temperature have increased while NO_x formation decreases. As previously mentioned, a good guess for its behavior could be related to local residence time variation by the increment in total

flow rate and then gases inlet velocities, which should be studied in more detail. The characteristics previously mentioned mean the power of the chamber has increased while its combustion has been more completed and cleaner which is also an advantage of this burner.

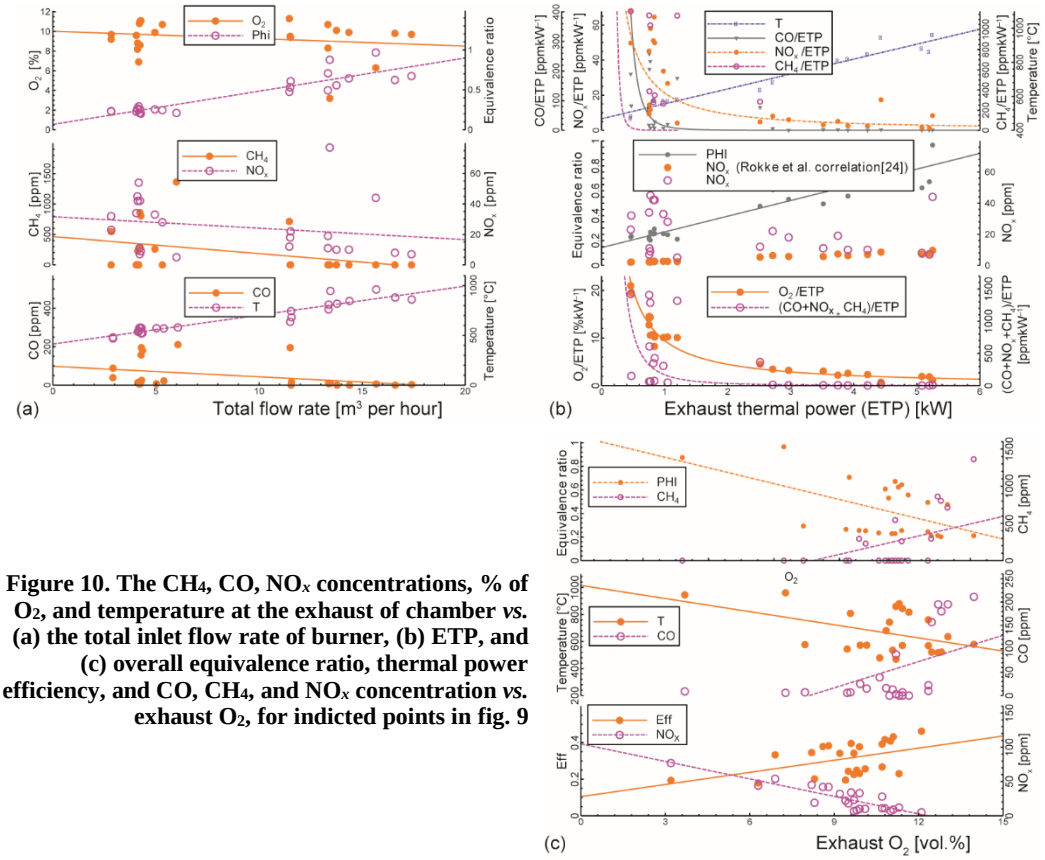

Figure 10. The CH_4, CO, NO_x concentrations, % of O_2, and temperature at the exhaust of chamber *vs.* (a) the total inlet flow rate of burner, (b) ETP, and (c) overall equivalence ratio, thermal power efficiency, and CO, CH_4, and NO_x concentration *vs.* exhaust O_2, for indicted points in fig. 9

It would be worthy if the measurements are presented based on the outlet power of this laboratory burner. To do that, a parameter entitled as exhaust thermal power (ETP) is defined:

$$\mathrm{ETP} = (\dot{m}_{\mathrm{air}} + \dot{m}_{\mathrm{fuel}})c_p(T_{\mathrm{outlet}} - T_{\mathrm{inlet}}) \tag{2}$$

In fig. 10(b), the pollutant generation per thermal power, burner overall equivalence ratio, exhaust gas temperature, excess oxygen per power unit, and NO_x contents are depicted *vs.* ETP. Moreover, NO_x generation in this burner is compared with the prediction of correlation (3) introduced by Rokke *et al.* [26].

$$\mathrm{NO}_x = 1.81P^{1.41}\dot{m}_{\mathrm{A}}^{0.3}q^{0.72} \tag{3}$$

They found this correlation very satisfactory for NO_x emissions from five different natural gas-fired industrial machines operating in the power range from 1.5 to 34 MW [27]. As can be seen, for the HFR region, there is a good agreement between the current measurements and also the equation prediction in which its accuracy is increased by power increment. That means the equation could be used for the current burner at high power loads, although it needs some

more tests. Furthermore, it may be concluded that the physical phenomena which lead to NO_x generation could be similar in this double swirl partially premixed burner and the mentioned large scale burners. The exhaust NO_x, CO, and UHC [ppmkW^{-1}] variation by power increment are also interesting according to the figure. They decrease by thermal power increment according to a *power law* distribution, while this reduction is faster for UHC and CO in comparison with NO_x. Thermal power increment is equivalent to linear growth of equivalence ratio and temperature, while excess oxygen per power unit decreases drastically from LFR to HFR region and marginally in the HFR zone. In other words, this behavior shows that NO_x emission generation decreases while the combustion inside the chamber is more completed for higher thermal power resulted from decrement in UHC, CO, and excess oxygen. Therefore, the mentioned characteristic could be a sign of the importance of residence time scale for NO_x formation in this burner. Summation on exhaust gas CO, UHC, and NO_x contents per power also indicate that the emission characteristics of this burner are different for LFR and HFR operating conditions, although both of them include the IRZ flow structure. For more information, the measured parameters are also depicted *vs.* the excess O_2 in fig. 10(c). It reemphasizes that the LFR and HFR operating conditions are different in terms of combustion emission and completing the combustion. Figure 10(c) indicates that the defined thermal efficiency is decreased by a reduction in excess oxygen, which could be attributed to higher thermal loss from burner structure.

As a whole, by considering all of the chemical species measurements and exhaust gas temperature, it can be concluded that there is a region with an ultra-low level of pollutants (*i. e.*, NO_x below 10 ppm) and complete combustion (*i. e.*, CO level lower than three ppm). This region is located approximately 25-50% above the LBO line in the HFR region in which there are significant high swirl induced effects and with a reasonable combustor outlet temperature. Therefore, reasonable burner operation conditions are discovered, which are the region with ultra-low pollutant levels and complete combustion. They include four operating conditions in a range of 8-12 kW and a global equivalence ratios of 0.57-0.69. These points of operating are important because they indicate the promising potential of current burner configuration for real applications

Effects of preheating

One of the ways to increase the efficiency of GT is to restore the heat from the turbine outlet. This heat can be used to preheat the air required in the combustion chamber and be useful for improving its stability. Given that the temperature of the outlet flow of GT is around 500 °C, by retrieving and directing this amount of heat towards the inlet of the combustion chamber, conditions can be made to preheat the air-flow up to at least 200 °C. Therefore, the effects of inlet air preheating on the performance and behavior of the combustion chamber can be attractive in terms of the efficiency of the cycle. In this way, here, the effects of a 100 °C air temperature increase on flame stability and pollutants are investigated.

Flame stability

Inlet air preheating effects on the LBO of the burner are followed in this subsection. Therefore, the LBO curves are shown for non-preheated and preheated conditions in fig. 11. It should be reminded that the related experiments are carried out in the best chamber configuration in terms of flame stability, which means in the presence of the wall and Injector (1). As can be seen, a 100 °C preheating of air-flow improves flame stability in the HFR region by 10%, although its effect in the LFR region is not tangible. This is similar to the flame response to some geometric parameters which were discussed before.

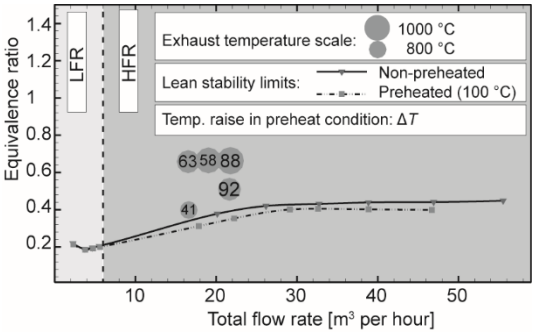

Figure 11. Exhaust mixture temperature under un-preheated condition and temperature raise due to preheating and two LBO curves for preheated and un-preheated conditions.

However, the improvement of flame stability in the HFR region can be discussed from different aspects and in terms of flame structure. According to the literature [1-3, 6], in high swirl flow burners, a re-circulation zone around the axis is present. This important swirl-induced structure has vital effects on stability and self-sustainability of flame by re-circulating hot combustion products to upstream and low-velocity zones where flame can be stabilized. Here for a constant inlet air mass-flow rate, air velocity to the chamber increases for about 30% as a consequence of inlet air preheating. Therefore it seems that velocity and pressure gradients and re-circulation zones would be strengthening which means that the conditions required for flame stability have been improved.

On the other hand, preheating has a positive effect on the flammability of combustible mixture as a result of increasing reactants' enthalpy level. It means that a mixture with higher initial energy is less susceptible to self-extinction-ignition sequence in comparison with the non-preheated mixture. This leads to more self-sustainability and stability behavior of the flame. It also may be worthy of mentioning that in current study temperature increment by about 100 K increases the kinematic viscosity of air stream by about 50% and velocity around 30% and, therefore, a reduction in Reynolds number would occur which will be helpful for relaminarization of flow. This effect may increase local residence time , which is compatible with requirements for stable combustion in terms of ignition delay time. Of course, this description, as a guess, competes with the preheating effect on the velocity field and should be studied locally in future works with more detailed data.

Exhaust temperature and NO_x

In this section, the effect of inlet air preheating on outlet temperature and NO_x emission is investigated for several operating conditions. In fig. 11, the exhaust mixture temperature in non-preheated condition and temperature increment due to preheating are shown. The size of the circles, according to the scale determined in the figure, shows the exhaust mixture temperatures in non-preheated conditions, and the numbers inside the circles show the exhaust mixture temperature increase due to preheating. As is shown in the figure, although the exhaust gas temperature is increased, this increment is less than the preheating level. Nevertheless, by increasing the inlet flow rate under constant equivalence ratio, the effect of preheating on the exhaust temperature has increased. That means by 22% increment in air-flow rate for a constant equivalence ratio, exhaust temperature increment due to the same preheating level is up to 40%. This temperature increase could be a result of excess enthalpy or heat release rate boosting or both of them. The NO_x production analysis helps this discussion. Moreover, in constant total flow rate, the temperature of the exhaust mixture increases as the global equivalence ratio approaches the stoichiometric limit, although this increment is not so severe at HFR. On the other hand, the preheating effect on temperature increment of exhaust gas has not changed substantially at HFR. For about 22 m^3 per hour, moving toward the stoichiometric condition not only increases temperature increment due to preheating but also decreases it from 92 K to 88 K. This

is relatively interesting, but it may be said that for a constant total flow rate, increment in equivalence ratio means a decrease in the air-flow rate. That means swirl induced structures may be weak as a result of lower inlet air velocities.

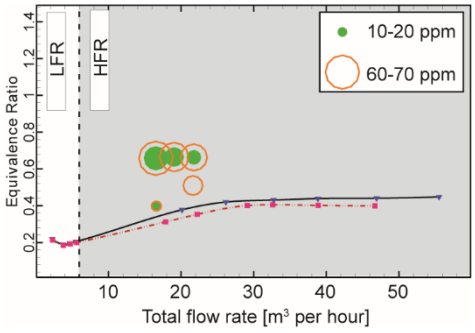

Figure 12. The NO_x level in un-preheated (filled circles) and preheated (empty circles) conditions and two LBO curves for preheated and un-preheated conditions

To follow the effect of preheating on NO_x formation, measured exhaust NO_x under non-preheated and preheated conditions are compared with each other in fig. 12. In this figure, the size of the rings shows NO_x levels for preheated conditions based on the determined scale, and solid circles represent the NO_x level under non-preheated conditions. It can be understood that for relatively constant equivalence ratio, NO_x production has been suppressed by total flow rate increment, although according to fig. 11, exhaust temperature has increased marginally. Moreover, this reduction is higher for non-preheated cases rather than the preheated cases. Because air-flow rate measurements are done before preheating, therefore under preheated condition, air inlet velocity is higher than non-preheated cases for a constant total flow rate, which means probably lower local residence time in reacting zones and distancing from NO_x favorable production condition. By reminding that NO_x decrease is in contradiction with exhaust temperature increment due to total flow rate increasing and also higher temperature increase at HFR for a constant preheating, it may be concluded that residence time is crucial under this condition. Therefore, preheating may compensate this deviation from the suitable conditions of NO_x production, which this description seems to be supported by observed behavior.

On the other hand, as mentioned, measured exhaust NO_x increases with preheating inlet air temperature. The NO_x level is 3-6 times more by about 100 K preheating. Reports on thermal NO_x show that the thermal NO_x production rate rapidly increases for temperature increase beyond 1800 K [28]. Therefore, it can be concluded that this behavior may be related to thermal NO_x generation increment in hot spots inside the chamber.

A comparison of preheating effects on NO_x formation at 18 and 22 m^3 per hour total flow rates shows that it is more effective at 22 m^3 per hour than 18 m^3 per hour. It is compatible with exhaust temperature behavior observed in fig. 11. That means for a higher flow rate, the temperature increase due to preheating has been higher. To get a more informative presentation, fig. 13 also follows the effects of preheating on exhaust gas temperature and NO_x content *vs.* the fuel-flow rate for the identified total equivalence ratios. By fuel-flow rate increment, temperature and also equivalence ratio are increased, but NO_x species behavior is different for low and high fuel-flow rates. That means although NO_x has increased by increasing the fuel-flow rate from around 0.22 to 0.38 m^3 per hour as well as exhaust gas temperature, it is suppressed for further increment in fuel-flow rate to 0.5. In contrast, the temperature and equivalence ratio have still increased. This behavior is not changed by air preheating and just shifted toward the higher NO_x levels.

In summary, these measurements revealed that limited preheating of air for double high swirl partially premixed burner could be helpful in terms of burner stability but has a negative impact on NO emission. This negative side effect of preheating is NO_x emission growth

in a range of 29-87%, while the measured ETP has increased in a range of 5% to 9%, respectively. To overcome this weakness, the burner improvement in lean extinction due to preheating, in the range of 10% could be considered by a further reduction in burner operating total equivalence ratio, which would be studied by the current research group. In this way, inlet air dilution seems to be a good solution, which should be considered precisely.

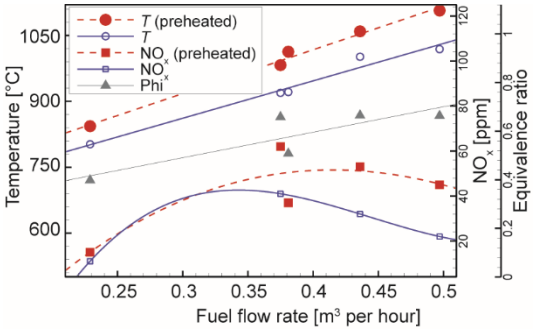

Figure 13. Measurements on SGTMC exhaust gas temperature and NO_x content and overall equivalence ratios for operating conditions identified in figs. 11 and 12

Conclusions

A GT model combustor with LPG fuel and air oxidizer was investigated experimentally in terms of combustion stability and pollutant generation. The burner LBO limit was extracted for different combustor configurations and preheating of inlet air. In this way, the effects of fuel injector type, burner casing, and 100 °C air preheating on LBO were analyzed. The results showed that the burner could operate properly under very lean conditions, especially during start procedure and low air-flow rates.

A comparison between the LBO limit of the current burner with LPG as fuel and the other reported tests with CH_4 fuel show that the LBO limit is similar which means the burner design and aerodynamic aspects are effective on the LBO of this burner rather than the fuel type

On the other hand, the LBO curve demonstrates different behavior in the HFR rather than the LFR. The injector input channels had favorable effect around 28% on stability limit, probably due to a better mixing in HFR. Besides this, confinement also had favorable crucial effects around 250% on LBO just in HFR. Moreover, according to performed parallel numerical simulations of the non-reacting flow field, both LFR and HFR regions had the same flow field structures, and vortex breakdown will be an effective mechanism on stability in both regions. Modeling revealed that swirl number at central air inlet is relatively constant by the increment in air-flow rate, although it increases for outer air inlet. Furthermore, for some flames with specified operating conditions, the effect of confinement on flame picture was analyzed in terms of some parameters such as width, height, side view surface, and flame root angle. The results showed that in LFR, flames have relatively the same shape and with increasing the flow rate, flame will become larger in all directions as expected. Moreover, as observed experimentally the flame was oscillatory with distributed luminosity and it was attached near the LBO at HFR.

Regarding the burner emissions, measurements showed that there is a region on stability graph with a good combustion efficiency and very low level of pollutants (*i. e.*, NO_x and CO concentration lower than 10 ppm and 3 ppm, respectively). This important region is located approximately 25-50% above the LBO. Moreover, in the studied operation envelope, increasing the total mass-flow rates results in power, overall equivalence ratio, and exhaust temperature increase while NO_x formation decreases. Analysis of emission per power unit shows that this parameter decreases drastically by thermal power increment of the burner.

It was also concluded that preheating inlet air-flow improves the lean stability behavior of flame up to 10%. However, preheating causes exhaust gas temperature increases, and thus NO_x production increases as an undesirable consequence around 3 to 6 times. Burner ETP and the parameter of NO_x emission per thermal power unit increase by inlet air preheating,

although the LBO limit is decreased. That means that simultaneously inlet air dilution and preheating may be a solution to regenerate heat with a reasonable emission production in this burner type.

Acknowledgment

The authors want to appreciate the help of Mr. Benyamin Asadi in the current research.

References

[1] Weigand, P., *et al.*, Investigations of Swirl Flames in a Gas Turbine Model Combustor: I. Flow Field, Structures, Temperature, and Species Distributions, *Comb. Flame*, *144* (2006), 1-2, pp. 205-224
[2] See, Y. C., Ihme, M., Large-Eddy Simulation of a Gas Turbine Model Combustor, *Proceedings*, 51st AIAA Aerospace Sciences Meeting, Grapevine, Tex., USA, 2013
[3] See, Y. C., Ihme, M., LES Investigation of Flow Field Sensitivity in a Gas Turbine Model Combustor, *Proceedings*, 52nd AIAA Aerospace Sciences Meeting, National Harbor, Md., USA, 2014
[4] Wankhede, M. J., *et al.*, Numerical Study of Unsteady Flow-Field and Flame Dynamics in a Gas Turbine Model Combustor, *Proceedings*, ASME Turbo Expo 2014, Dusseldorf, Germany, pp V04AT04A050-V04AT04A50
[5] See, Y. C., Ihme, M., Large Eddy Simulation of a Partially-Premixed Gas Turbine Model Combustor, *Proc. Comb. Inst*., *35* (2015), 2, pp. 1225-1234
[6] Mardani, A., Fazlollahi-Ghomshi, A., Numerical Investigation of a Double-Swirled Gas Turbine Model Combustor Using a RANS Approach with Different Turbulence-Chemistry Interaction Models, *Energy Fuels*, *30* (2016), 8, pp. 6764-6776
[7] Stohr, M., *et al*., Experimental study of Vortex-Flame Interaction in a Gas Turbine Model Combustor, *Comb. Flame*, *159* (2012), 8, pp. 2636-2649
[8] Widenhorn, A., *et al.*, Numerical Characterization of a Gas Turbine Model Combustor Applying Scale-Adaptive Simulation, *Proceedings*, ASME Turbo Expo, Orlando, Fla., USA, 2009, pp 11-23
[9] Duan, X. R., *et al*., Experimental Investigations and Laser Based Validation Measurements in a Gas Turbine Model Combustor, *Prog. Comput. Fluid Dy*, *4* (2004), 3-5, pp. 175-182
[10] Weigand, P., *et al*., Laser Diagnostic Study of Mechanism of a Periodic Combustion Instability in a Gas Turbine Model Combustor, *Flow, Turb. Comb.*, *75* (2005), 1-4, pp. 275-292
[11] Meier, W., *et al.*, Reaction Zone Structures and Mixing Characteristics of Partially Premixed Swirling CH_4/Air Flames in a Gas Turbine Model Combustor, *Proc. Comb. Inst*., *30* (2005), 1, pp. 835-842
[12] Meier, W., *et al*., Investigation of Swirl Flames in a Gas Turbine Model Combustor: II-Turbulence-Chemistry Interactions, *Comb. Flame*, *144* (2006), 1-2, pp. 225-236
[13] Sadanandan, R., *et al*., Simultaneous OH-PLIF and PIV Measurements in a Gas Turbine Model Combustor, *Appl. Phys. B*, *90* (2008), 3-4, pp. 609-618
[14] Stohr, M., *et al*., Experimental Study of Unsteady Flame Structures of an Oscillating Swirl Flame in a Gas Turbine Model Combustor, *Proc. Comb. Inst.*, *32* (2009), 2, pp. 2925-2932
[15] Sadanandan, R., *et al.*, Flow Field-Flame Structure Interactions in an Oscillating Swirl Flame, *Comb. Explos. Shock Waves*, *45* (2009), 5, pp. 518-529
[16] Boxx, I., *et al*., Investigation of a Gas Turbine Model Combustor by Means of High-Speed Laser Imaging, *Proceedings*, 47th AIAA Aerospace Sciences Meeting, Orlando, Fla, USA, 2009
[17] Boxx, I., *et al*., Sustained Multi-kHz Flame Front and 3-Component Velocity-Field Measurements for the Study of Turbulent Flames, *Appl. Phys. B*, *95* (2009), 1, pp. 23-29
[18] Boxx, I., *et al*., Temporally Resolved Planar Measurements of Transient Phenomena in a Partially Pre-Mixed Swirl Flame in a Gas Turbine Model Combustor, *Comb. Flame*, *157* (2010), 8, pp. 1510-1525
[19] Steinberg, A. M., *et al*., Flow-Flame Interactions Causing Acoustically Coupled Heat Release Fluctuations in a Thermo-Acoustically Unstable Gas Turbine Model Combustor, *Comb. Flame*, *157* (2010), 12, pp. 2250-2266
[20] Stohr, M., *et al*., Dynamics of Lean Blow-Out of a Swirl-Stabilized Flame in a Gas Turbine Model Combustor, *Proc. Comb. Inst.*, *33* (2011), 2, pp. 2953-2960
[21] Kutne, P., *et al*., Experimental Analysis of the Combustion Behavior of Oxyfuel Flames in a Gas Turbine Model Combustor, *Proc. Comb. Inst*., *33* (2011), 2, pp. 3383-3390

[22] Allison, P. M., *et al*., Acoustic Behavior of a Partially-Premixed Gas Turbine Model Combustor, *Proceedings*, 50th AIAA Aerospace Sciences, Nashville, Tenn., USA, 2012
[23] Allison, P. M., Experimental Characterization of Combustion Instabilities and Flow-Flame Dynamics in a Partially-Premixed Gas Turbine Model Combustor, Ph. D. thesis of Philosophy (Aerospace Engineering), The University of Michigan, En Arbor, Mich., USA, 2013
[24] Williams, T. C., *et al.*, Idealized Gas Turbine Combustor for Performance Research and Validation of Large Eddy Simulations, *Review of Scientific Instruments, 78*, (2007), ID 035114
[25] Lu, G., *et al.*, Vision Based Monitoring and Characterisation of Combustion Flames, *Journal of Physics: Conference Series, 15* (2005), 1, pp. 194-200
[26] Rokke, N. A., *et al*., Pollutant Emissions from Gas Fired Turbine Engines in Offshore Practice – Measurements and Scaling, *Proceedings*, Int. Gas Turbine and Aeroengine Congress and Exposition, Cincinati, O., USA, No. 93-GT-170, 1993
[27] Lefebvre, H., *et al*., *Gas Turbine Combustion-Alternative Fuels and Emissions*, 3rd edition, Taylor and Francis Group, LLC, New York, USA, 2010
[28] ***, *An introduction to combustion Concepts and Applications*, S. R. Turns, 2nd edition, McGraw-Hill, New York, USA, 2000

Paper submitted: June 23, 2019
Paper revised: March 6, 2020
Paper accepted: March 12, 2020